FILAMENTS IN THE RADIO LOBES OF M87

DEAN C. HINES
Physics Department and Astrophysics Research Center, New Mexico Institute of Mining and Technology

FRAZER N. OWEN
National Radio Astronomy Observatory[1]

AND

JEAN A. EILEK
Physics Department and Astrophysics Research Center, New Mexico Institute of Mining and Technology

ABSTRACT

We present a total intensity VLA image of the inner lobes of M87 at 6 cm. The map has a resolution of $0\overset{''}{.}4$ and a dynamic range of $\sim 10^5$. We find several bright features—loops and filaments—within the lobes. These features appear to be overpressure compared to the surrounding gas. We consider several possible origins for these filaments. We show that cooling instabilities cannot account for the features. Resistive instabilities are also unlikely unless *in situ* particle acceleration is occurring. Transonic turbulence or shocks in the lobes might be the most likely explanation of the features.

Subject headings: galaxies: individual (M87) — galaxies: structure — interferometry — radio sources: galaxies

I. INTRODUCTION

Over the past few decades the giant elliptical galaxy in the Virgo cluster, M87 (also designated 3C274, NGC4486, Virgo A), has become a prime laboratory for the study of active galaxies. The peculiar nature of M87 was first noticed by Curtis (1918) with the discovery of the optical jet. Optical observations show the jet to be highly linearly polarized with no detectable emission lines, suggesting that the emission is synchrotron (Burbidge 1956). The jet has been resolved into several emission features, designated A-I in order of decreasing brightness (Neito and Lelievre 1982 and references therein).

X-ray observations show that M87 sits in the center of an envelope of hot gas (e.g., Canizares et al. 1979; Lea, Mush-otzky, and Holt 1982, Stewart et al. 1984) which is a thermal bremsstrahlung source. The short bremsstrahlung cooling times in this gas, and the cooler temperatures in the inner regions, suggest a cooling flow in the inner ~ 60 kpc of this gas (e.g., Canizares et al. 1982; White and Sarazin 1988). Optical line emission from clouds or filaments is seen in the inner few kpc of this gaseous halo (Ford and Butcher 1979; Owen and Keel 1989). We take the distance to the system to be 17 Mpc, which means that $1''$ corresponds to 81 pc at the source.

The galaxy was first identified as a strong radio source by Baade and Minkowski (1954). M87 is a core-halo, Fanaroff-Riley type I radio source (Fanaroff and Riley 1974). The halo extends to $\sim 12'$ from the nucleus (Andernach et al. 1979; Fei-gelson et al. 1987). The inner radio core is $\sim 1\overset{'}{.}5 \times 2\overset{'}{.}0$ and can be divided into four regions of emission: the nucleus, the jet, the North Preceding (Np) lobe, and the South Following (Sp) lobe (Turland 1975; Forster 1980).

The radio properties of the jet have been extensively studied (Turland 1975; Laing 1980; Owen, Hardee, and Bignell 1980; Biretta, Owen, and Hardee 1983; and Owen, Hardee, and Cornwell 1989, hereafter OHC). These observations show that the radio emission corresponds well with the optical jet, that the jet is continuous (rather than a sequence of discrete knots) and that the emission is probably from the surface of the jet (OHC). Recent proper motion observations of Biretta, Owen, and Cornwell (1989) find subluminal motion $\sim 0.3c \pm 0.2c$ for knot A, the brightest knot in the jet. The nucleus has been studied with VLBI on milliarcsec scales (Schmitt and Reid 1985; Spencer and Junor 1986; Reid et al. 1989). These observations indicate that the jet material must collimate less than 1 pc from the central engine, and that the ejection of the material must occur on scales less than 0.01 pc. They also measure a velocity $\sim 0.3c$ in the milliarcsecond jet.

In this paper, we present new radio observations of the core source in M87. The observations use new data reduction techniques to yield extremely high quality images of the radio structure. We have found previously undetected structures in both the Np and Sf radio lobes. These structures are reminiscent of the filaments seen in some Fanaroff-Riley type II double sources such as Cyg A (Perley, Dreher, and Cowan, 1984), and in some wide-angle tailed sources such as $1159+583$ (O'Donoghue 1989), although the features in M87 do not appear as ordered as in other sources. After describing the observations, we present basic properties of the brighter features, and then consider possible formation mechanisms for the features. We find that thermal instabilities will not account for the bright features in the M87 environment. We are led to suggest that the features arise either from strong turbulence or shocks, or both, or possibly from tearing mode instabilities in the relativistic plasma. In this latter case, *in situ* acceleration must be occurring in order to maintain the synchrotron luminosity of the features.

II. OBSERVATIONS

We observed M87 on 1986 April 25, using the VLA at 6 cm in the A array (Thompson et al. 1980). In order to improve (u, v) coverage, we used the ability of the VLA to measure four different frequencies simultaneously, to construct a bandwidth synthesis image (Braun, Gull, and Perley 1987; Wilkinson,

Conway, and Biretta 1987). We observed M87 for a full 12 hr period at 4.635, 4.735, 4.835, and 4.935 GHz each with a 50 MHz bandwidth. In principle, spectral index gradients over the source can limit the dynamic range of a bandwidth synthesis image. In practice, this problem is usually negligible unless the gradient is very large; the errors introduced are proportional to the difference in sidelobes at the different frequencies (0.1, typically), the differential spectral index, and the fractional bandwidth (Conway, Cornwell, and Wilkinson 1989). In the present case, these errors were comparable to the thermal noise for the observation and limit the dynamic range to a few times 10^5 (where dynamic range is the ratio of the peak flux density to off-source rms noise). To reduce the instrumental errors, we reset the antenna delays just prior to the observations to minimize closure errors caused in part by delay drift.

The absolute flux densities for M87 were calibrated by observing the primary calibrator, 3C286, for 5 minutes at each frequency at the beginning and the end of the run. The observed flux density of 3C286 was calibrated using the Baars scale (Baars et al. 1977). The secondary calibrator 1252+119 was observed for 1 minute every 20 minutes to track phase errors caused by changing atmospheric conditions over the array. The raw data were calibrated in the standard way using ANTSOL to calculate the antenna gain corrections (Thompson et al. 1980). The gain corrections based on the 3C286 data were applied to both M87 and 1252+119 data. Then 1252+119 was used to calibrate the antenna polarization and the antenna based gains for the M87 data.

All data reduction was performed on a VAX 11/780 using NRAO's AIPS software package. Since our goal was to produce a total intensity image with the highest dynamic range possible, we were very concerned with errors on the order of a few tenths of a per cent. The standard reduction procedure usually yields images with only $\sim 10^3$ dynamic range. But the

VLA is theoretically capable of producing images with dynamic range $\sim 10^6$. The problem lies in instrumental errors and in baseline dependent gains.

The standard data reduction procedure employs several iterations of the Clark (1980) implementation of the CLEAN algorithm (Hogbom 1974) and self-calibration (Pearson and Readhead 1984). However, self-calibration corrects only for antenna based effects, and this only reduces errors to a few per cent. There are also baseline dependent effects that must be corrected. At the VLA, these corrections (called closure corrections) can be applied using BCAL1 and BCAL2 in AIPS (Walker, Benson, and Unwin 1987). We note that the baseline gains may vary in time. BCAL uses a time-averaged offset for each baseline calibration, so some residual errors may still persist (e.g., the concentric rings around the point source in Figures 2, 3, and 4 below).

To calculate the closure corrections for M87, we imaged the primary calibrator 3C286 as accurately as possible. This was accomplished by successive iterations of CLEANing and self-calibration. The data taken at 4.635 GHz were processed first to get a reasonable model for self-calibration of the other three frequencies. When each of the four 3C286 data sets had converged on a solution, the data were combined to yield the total intensity image shown in Figure 1 (where the dynamic range is $\sim 25,000$). Each image of 3C286 was used to calculate the closure corrections for each frequency of the M87 data.

The 4.635 GHz data for M87 were imaged with several iterations of CLEAN and self-calibration. The resulting image was used as the beginning model for self-calibrating the other three frequencies. After each data set had converged to a reasonable solution, the data were combined to give a single data base containing $\sim 1,200,000$ visibility records. This combined data base was processed through several more iterations of CLEAN and self-calibration.
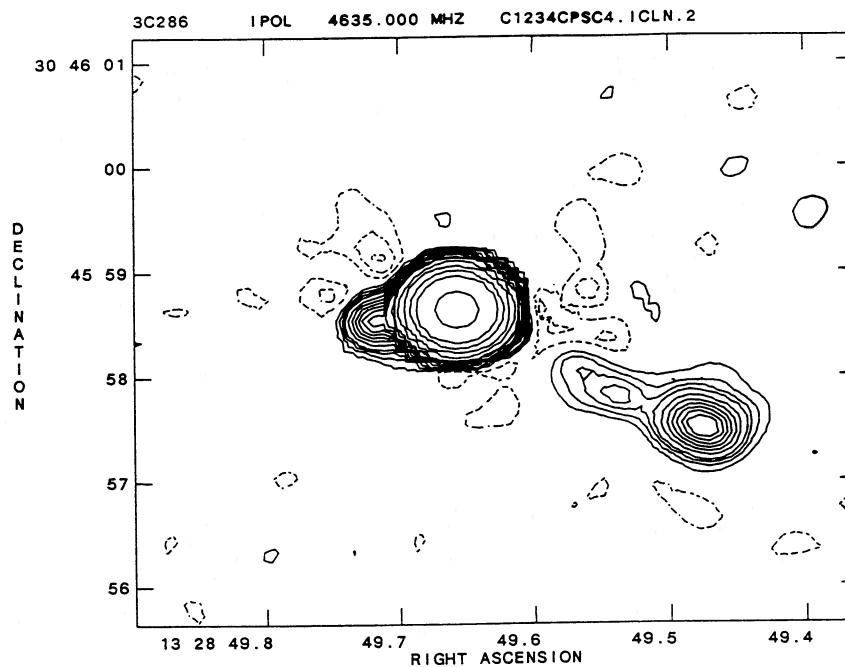

FIG. 1.—Total intensity image of the primary calibrator 3C286 at 6 cm. The dynamic range is $\sim 25,000$. The negative "holes" are caused by residual phase errors. This image was used to calculate the baseline closure errors for the M87 image. Contour intervals are $(-3, -2, -1, 1, 2, 3, 4, 6, 8, 10, 12, 14, 16, 20, 30, 40, 80, 160, 400, 800, 4040) \times 0.123$ mJy per beam.
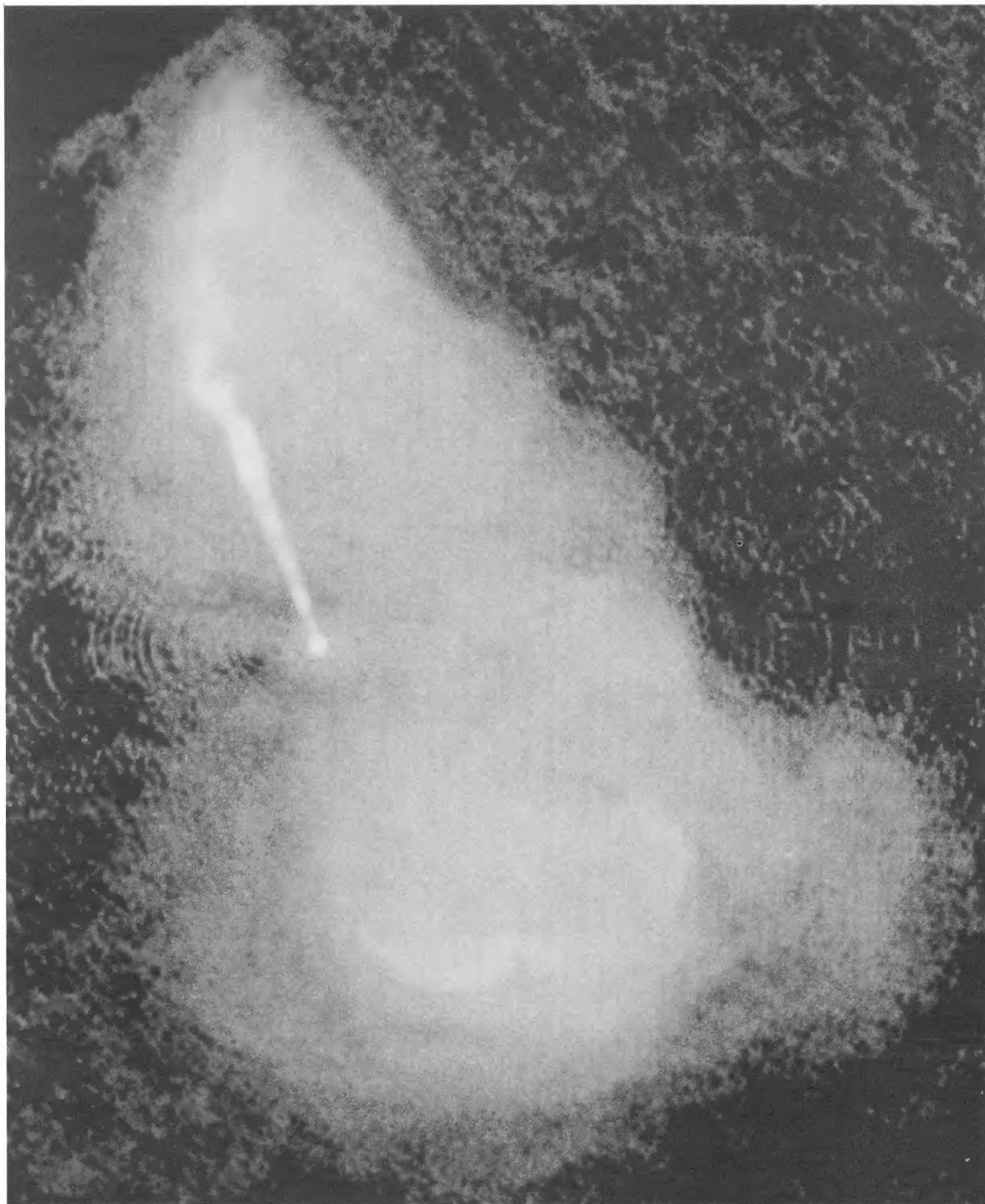
PLATE 7

FIG. 2.—Total intensity image of M87. The image was deconvolved using the maximum entropy method with a heavily tapered 20 cm image as the default model. The image is displayed with a logarithmic transfer function.

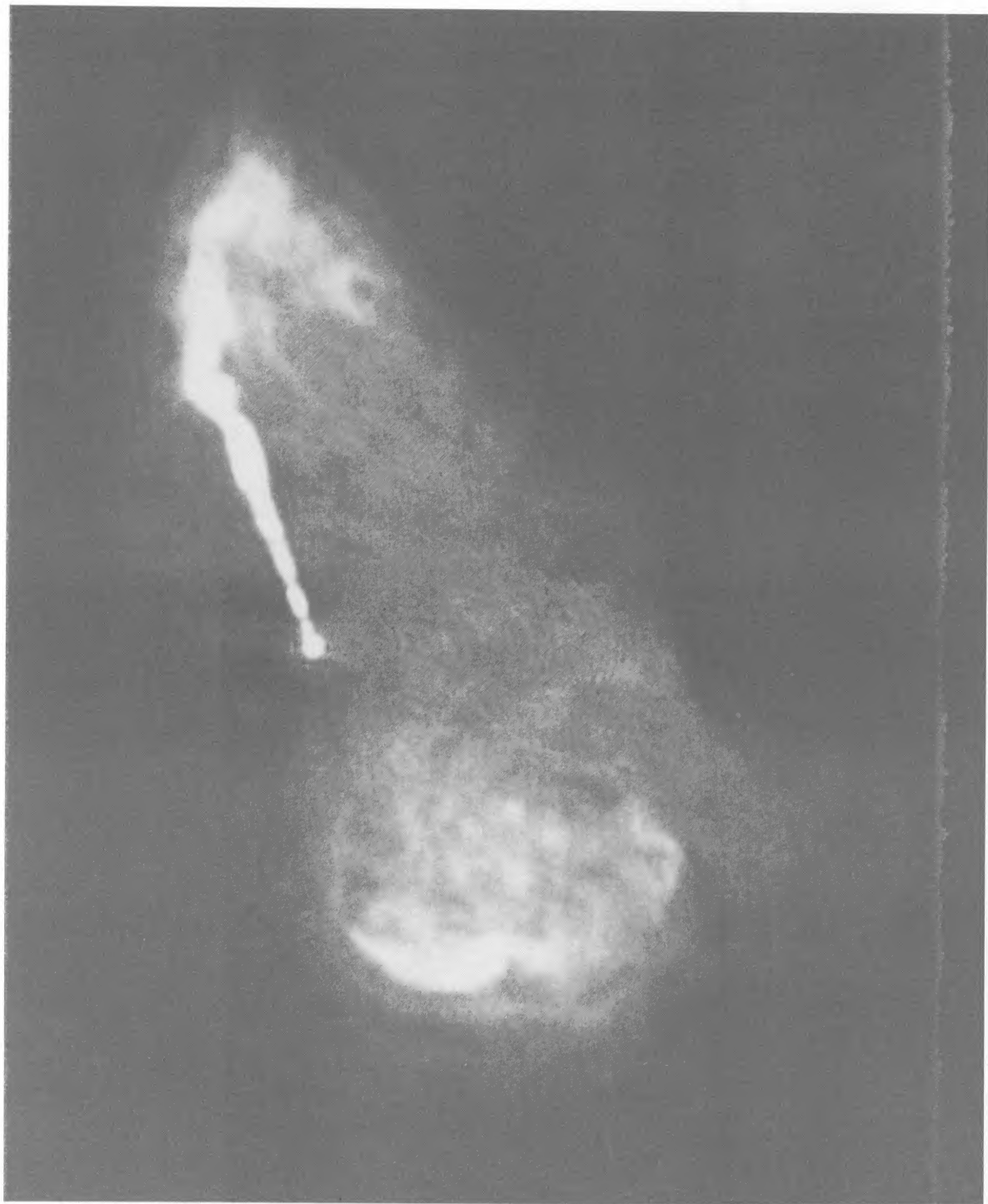HINES *et al.* (*see* **347**, 714)

PLATE 8

Fig. 3.—Total intensity image of M87 (the same image as in Fig. 2). The transfer function (a combination of histogram equalization and a logarithm) is set to enhance the features embedded in the diffuse emission.

HINES et al. (see **347**, 714)

To arrive at the final image, 3 hr of C array data at 6 cm were added to fill in short-spacing flux. The final deconvolution was performed using the Maximum Entropy Method ("MEM"; VTESS in AIPS). MEM was used because CLEAN had trouble converging on a solution that was consistent with both the fine filamentary structure and the diffuse emission in the source. Prior to deconvolution with VTESS, the dirty image was convolved with a $0\farcs4$ circular Gaussian to obtain the proper units and avoid hyperresolution (Cornwell 1986). For the initial model for the MEM deconvolution, we used a heavily tapered, 20 cm A array image of the region. This allowed much better convergence than the standard default (flat) initial model (Cornwell 1986). The cell size of the tapered image was carefully adjusted to match the 6 cm cell size ($0\farcs19$ pixel^{-1}). Deconvolution was performed until the MEM algorithm had converged to a solution consistent with a noise level ~ 22 μJy beam^{-1}. The resulting total intensity image has a dynamic range $\sim 1.5 \times 10^5$.

III. RESULTS

Figure 2 (Plate 7) shows the final total intensity image of the inner radio core of M87. The physical scale of the source ~ 5 kpc end to end. The image is displayed with a logarithmic transfer function. The jet, the nucleus, and the inner Np and Sf radio lobes are clearly visible. In addition, there are several previously undetected features embedded in the diffuse lobe emission. Figure 3 (Plate 8) shows the same image with a transfer function chosen to emphasize the embedded features. Figure 4 is a contour image of the region showing the locations of bright features which we label and discuss below.

a) Structure within the Inner Lobes

In both Figures 2 and 3, one easily picks out what look like rings, wisps, and filaments; the inner lobes are certainly not uniformly filled with radio luminous plasma. We have picked out the brightest and most easily identifiable of these features for the following analysis. We list these in Table 1, choosing Greek letters to identify them, to avoid confusion with the labeling of knots in the jet. For each of the labeled features, Table 1 lists the approximate position of the feature in 1950.0 coordinates, the estimated flux density, the estimated volume (see discussion below) and the volume emissivity. Most of these features are well resolved (i.e., a few beam widths across); in cases where the feature is barely resolved, the dimensions were calculated using the method of Burns, Owen, and Rudnick (1979). The radio luminosity of each feature was calculated assuming that the spectrum is a power law, $S_\nu \propto \nu^{-\alpha}$ with $\alpha = 0.6$, extending from 10^7 Hz to 10^{11} Hz.

There are three prominent features in the Np lobe. Feature α is just beyond (away from the nucleus) knot B in the jet. At this point, the emission splits into two linear strings which intersect and separate again further west of knot B. The strings are only slightly resolved (at FWHM $\sim 0\farcs5$), with a maximum separation of $1\farcs2$. Each of the strings is listed separately in Table 1. Both features β and γ are curved regions of emission that could be either loops or shell-like features. Each has a projected radius of curvature of $1\farcs5$. Table 1 lists these features twice, allowing for each possible geometry.

There are several features in the Sf lobe. Features δ, ϵ, and ζ are each round emission regions with average FWHM $\sim 1\farcs7$. These three features were assumed to be filled spheres of emis-
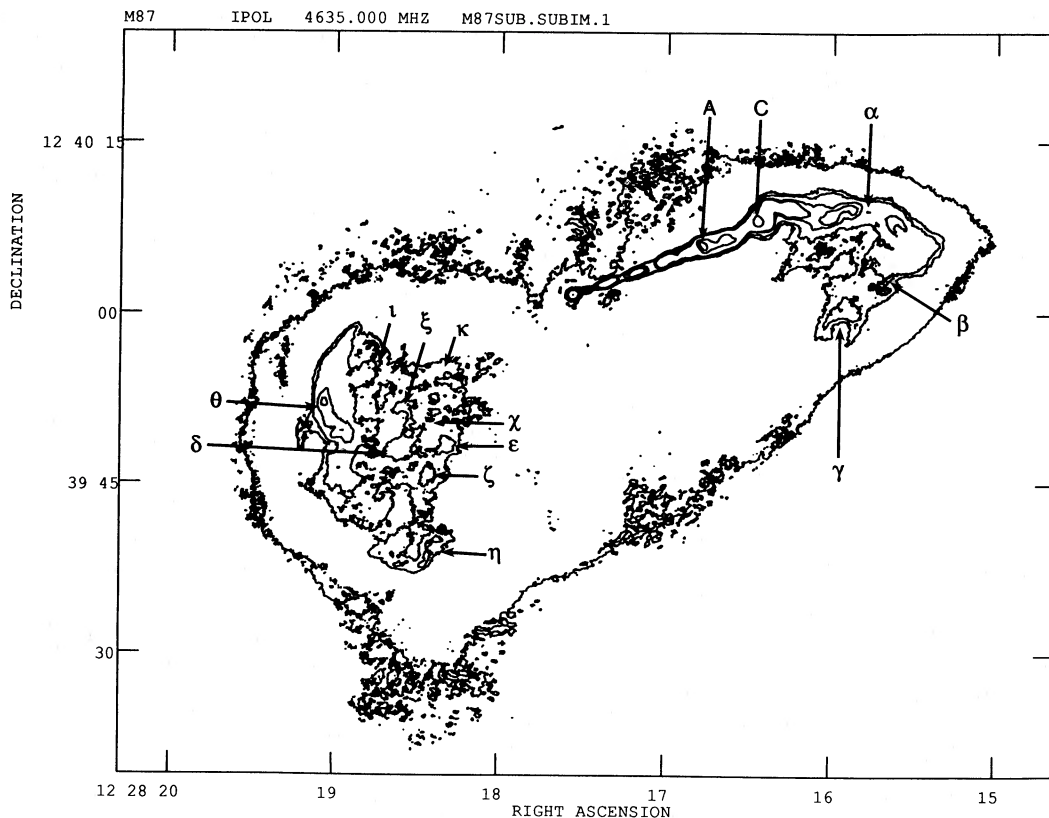

FIG. 4.—Contour representation of the M87 image in Figs. 2 and 3. Contour intervals are (1.0, 4, 5, 6, 10, 50, 100, 1634) × 0.38 mJy per beam.

HINES, OWEN, EILEK

TABLE 1

Observed Properties of Features

Feature	R.A.	Decl.	S(mJy)	V(cm^3)	j(ergs s^{-1} cm^{-3})
α_{upper}	122815.6	124008.3	42.5	2.6×10^{61}	2.3×10^{-23}
α_{lower}	122815.6	124007.4	57.0	3.9×10^{61}	3.3×10^{-23}
β_{shell}	122815.7	124004.3	66.9	1.6×10^{62}	5.9×10^{-24}
β_{loop}	122815.7	124004.3	52.1	1.5×10^{62}	4.9×10^{-24}
γ_{shell}	122815.9	123969.1	211	4.1×10^{62}	7.3×10^{-24}
γ_{loop}	122815.9	123969.1	180	1.6×10^{62}	1.6×10^{-23}
δ	122818.6	123948.1	43.1	4.5×10^{61}	1.4×10^{-23}
ϵ	122818.3	123948.3	32.7	2.4×10^{61}	1.9×10^{-23}
ζ	122818.4	123945.5	23.4	7.9×10^{60}	4.2×10^{-23}
η	122818.5	123939.0	200	3.1×10^{62}	9.0×10^{-25}
θ	122819.0	123951.3	898	3.3×10^{63}	3.9×10^{-24}
ι	122818.7	123955.3	168	5.7×10^{62}	4.2×10^{-24}
κ	122818.3	123954.1	83.7	7.0×10^{61}	1.7×10^{-23}
ξ	122818.5	123950.3	19.5	9.3×10^{60}	2.9×10^{-23}
χ	122818.3	123950.3	18.6	9.3×10^{60}	2.8×10^{-23}
Bg	122817.3	123950.0	1.21	9.2×10^{61}	6.5×10^{-25}

sion in Table 1; we note, however, that these features appear to have a "C" shaped geometry at 2 cm (OHC), which may suggest a more complex geometry. Feature η is the curved string of emission just below features δ, ϵ, and ζ. Each bend has a radius of curvature of 1″.5. Feature θ was previously resolved in the observations of Biretta, Owen, and Hardee (1983), and it is by far the dominant feature in the Sf lobe. We discuss feature θ in a bit more detail below (§ IIIb). Feature ι resembles features β and γ in the Np lobe. It lies near the top of θ and may be physically associated with θ. Its radius of curvature is 1″.5. Feature κ is composed of at least three loops of emission, which may or may not be physically associated. Each loop has a radius of curvature of 1″.5. The numbers presented in Tables 1 and 2 apply only to the brightest (easternmost) loop. Features ξ and χ are linear emission regions that extend radially from the vicinity of δ. These last six features—η, θ, ι, κ, ξ, χ—were all assumed to be filled cylinders lying in the plane of the sky, with dimensions taken directly from the image.

We note that the simplest likely geometries were assumed in describing all of the features. No attempt has been made to take projection into account. Further, while the spherical features could of course be cylinders seen end-on, and the linear features could be sheets seen edge-on, no such complications were assumed in calculating the values presented in Table 1.

TABLE 2

Minimum Pressure Analysis

Feature	$B(\mu G)$	p_{min}(dyn cm^{-2})	t_{sy}(yr)
α_{upper}	86	6.2×10^{-10}	8.2×10^{5}
α_{lower}	84	5.9×10^{-10}	8.5×10^{5}
β_{shell}	58	2.8×10^{-10}	1.5×10^{6}
β_{loop}	56	2.6×10^{-10}	1.6×10^{6}
γ_{shell}	62	3.2×10^{-10}	1.3×10^{6}
γ_{loop}	77	5.0×10^{-10}	9.7×10^{5}
δ	74	4.6×10^{-10}	1.0×10^{6}
ϵ	82	5.7×10^{-10}	8.8×10^{5}
ζ	100	8.8×10^{-10}	6.3×10^{5}
η	66	3.7×10^{-10}	1.2×10^{6}
θ	52	2.2×10^{-10}	1.8×10^{6}
ι	53	2.3×10^{-10}	1.7×10^{6}
κ	79	5.2×10^{-10}	9.4×10^{5}
ξ	93	7.2×10^{-10}	7.3×10^{5}
χ	91	7.0×10^{-10}	5.3×10^{5}
Bg	22	4.0×10^{-11}	4.4×10^{6}

We did explore this possiblity in some detail for the bright feature θ in the Sf lobe. One might argue that this feature is not a linear filament, but rather a luminous shell around the eastern edge of the lobe. For instance, such a shell might be due to the interaction of an invisible "counterjet" with the ambient medium. We explored this possibility by calculating surface brightness profiles from a hemisphere of low emissivity plasma surrounded by a shell of higher emissivity plasma. Figure 5 shows the surface brightness for two cuts through the Sf lobe, including feature θ. This can be compared with Figure 6 which shows several simulated brightness profiles for the spherical shell, for various shell thickness and emissivity ratios. We see that the simulations do not match the data well. We conclude that θ is probably a discrete, cylindrical feature.

In addition to these labeled features, there are other regions of enhanced brightness in both the Np and Sf lobes that could be physical features as well. We have, however, listed only the brightest features which we are reasonably sure are likely to be real structures.

Finally, the numbers for the background (Bg) were derived assuming a pencil beam with diameter $\simeq 0″.4$ and length $30″$. The volume emissivity was estimated by measuring the flux density ($S = 1.2$ mJy beam^{-1}) in a region of the source free from obvious filaments, and assuming that this value represents the background, interfilament gas.

b) Minimum Pressure Analysis of These Features

Assuming that the observed radio emission from the inner radio lobes is synchrotron emission, we can derive minimum pressures and minimum-pressure magnetic fields from the observed flux densities and assumed volumes (Burns, Owen, and Rudnick 1979; O'Dea and Owen 1987). These numbers are listed for each feature in Table 2, along with the lifetime of particles which radiate at 5 GHz under these conditions. We have assumed a uniformly filled volume (that is, a filling factor of unity) and that there is equal energy in ions and electrons (so that the usual factor $k = 1$). We again assumed a spectral index of $\alpha = 0.6$ and a frequency range of 10^7–10^{11} GHz.

An important question is how these minimum pressures compare with the pressure in the X-ray emitting thermal gas which surrounds the radio source. We follow OHC, who estimated the conditions in the inner few kpc of the X-ray gas using the models of White and Sarazin (1988), scaled to our

M87   IPOL   4635.000 MHZ   M87SUB.SUBIM.1

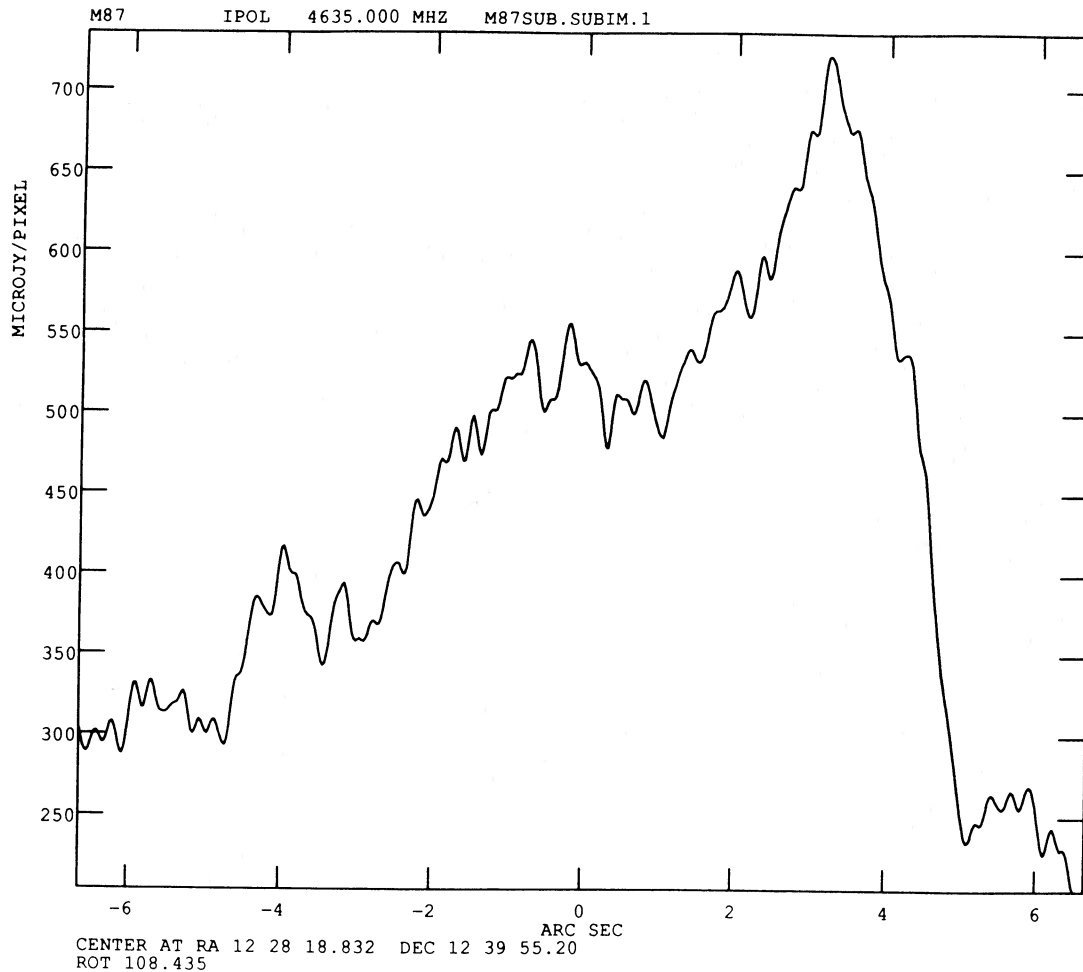CENTER AT RA 12 28 18.832   DEC 12 39 55.20
ROT 108.435

FIG. 5a

FIG. 5.—Surface brightness for two cuts through the Sf lobe, centered at (slice a) $\alpha = 122818.8$, $\delta = 123955.2$, and (slice b) $\alpha = 122818.8$ and $\delta = 123950.8$. Slice (a) begins in the middle of the lobe, has the same position angle as the jet, and passes through feature θ. Slice (b) begins in the same place and passes through the brightest part of feature θ.

assumed distance of 17 Mpc. The White and Sarazin models are spherically symmetric models of a cooling inflow, at a rate ~ 20–$30~M_\odot~\mathrm{yr}^{-1}$, inside of ~ 60 kpc; the inflow rate is an increasing function of distance in these models. Between 0.7 and 2 kpc, OHC take the pressure of the ambient thermal gas to be $p_x \sim 5.1 \times 10^{-10} z_{\mathrm{kpc}}^{-0.35}$ dyn cm^{-2}. (OHC note that scaling to 17 Mpc amounts to multiplying the pressure and density in the White and Sarazin models by a factor of 1.2 and decreasing the linear scale by a factor of 0.7). The projected distance of the labeled features from the core ranges from 1.0 to 2.3 kpc; the thermal gas pressure in this region, from the OHC relation, ranges from 3.7×10^{-10} to 5.0×10^{-10} dyn cm^{-2}. From Table 2, we see that six of the 12 labeled features (α_{upper}, α_{lower}, β, γ, ξ, ζ, and χ) appear to be overpressure by a factor of 2 or more. We note that some of the features (α_{upper}, α_{lower}, ξ, χ) are only partially resolved, so that their true minimum pressure may be greater than that listed in Table 2. Also, these p_{min} values were calculated assuming that the ratio of ion pressure to electron pressure, $k = 1$; any increase in k, whether from relativistic ions or thermal gas, will also increase p_{min} over the values in the table.

Further, we recall that any deviation from the minimum-pressure condition [in which $p_{\mathrm{rel}} = (4/3)p_B$] will result in the true pressure exceeding p_{min}. We show this behavior in Figure

7, in which we plot the total (relativistic plus magnetic) pressure in a bright filament.

$$p_{\mathrm{tot}} = \frac{(1+k)}{3} c_{12} \frac{L}{V} \frac{1}{B^{3/2}} + \frac{B^2}{8\pi}, \qquad (1)$$

as a function of the magnetic field in the filament. (Here, L is the total luminosity, V is the total volume and c_{12} is a numerical constant. We have assumed a uniformly filled feature and have related the relativistic particle pressure to the magnetic field, luminosity and volume by $p_{\mathrm{rel}} = \frac{1}{3}(1+k)c_{12} L/VB^{3/2}$; see Pacholczyk 1970). We picked our bright feature to have a minimum-pressure magnetic field of 100 μG. We also indicate the range of the thermal gas pressure, from OHC; this is below any allowed value of the pressure in the feature.

Now, a factor of 2 difference between the minimum pressure inferred from the radio data and the thermal gas pressure inferred from cooling-flow deconvolutions of the X-ray data may not be enough to force one to the conclusion that the luminous features cannot be pressure confined. However, the caveats listed above, along with some theoretical arguments on the possible origins of the filaments (§§ IV and V, below) lead us to suspect that the features are, indeed, strongly over-pressure with respect to the surrounding thermal gas.
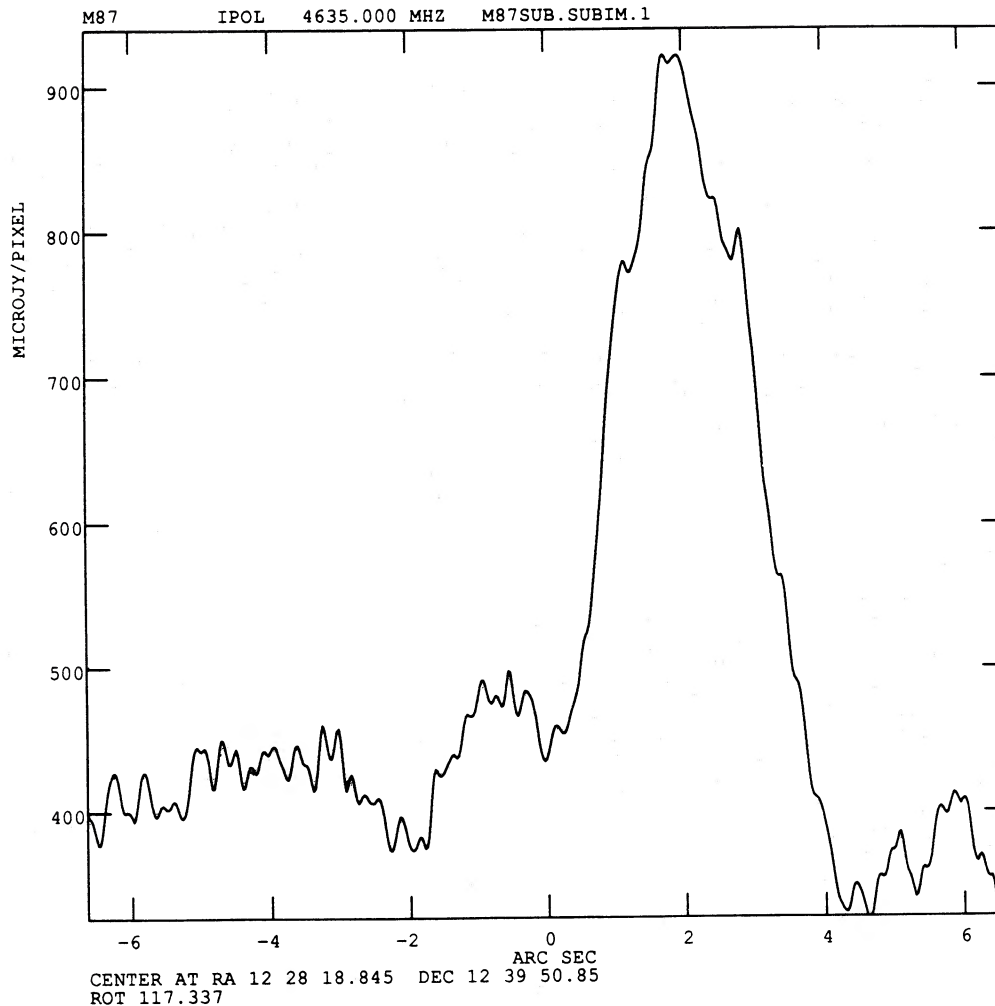
Fig. 5b

Finally, we note that the minimum pressure for the background plasma in the radio lobes is well below p_x, so that our data is consistent with that plasma being confined by the pressure of the surrounding thermal gas.

IV. THE NATURE OF THE FEATURES WITHIN THE LOBES

The striking result of these observations is the discovery that the inner lobes of M87 are not uniformly filled with luminous plasma. Rather, a wealth of substructure is seen; the eye picks out luminous filaments or clouds within a diffuse, low-surface brightness background. In § III we labeled and measured the brighter of these features; other structures, at a lower contrast to the background, can also be picked out in the images. These luminous features are reminiscent of the bright linear filaments found in other extended radio sources such as Cyg A (Perley, Dreher, and Cowan, 1984) or 1159+583 (O'Donoghue 1989), although the features in M87 are not as clearly linear and ordered as those in these other, larger objects.

Any discussion of the features must address two important points: the higher emissivity and the geometry of the features. The monochromatic synchrotron emissivity from a power-law electron spectrum [that is, $N(E) = N_0 E^{-s}$ for $E > E_{min}$] can be written (e.g., Pacholczyk 1970),

$$j_{sy}(v) = Cn_{rel} \bar{E}^{(s-1)} B^{(s+1)/2} v^{-(s-1)/2} . \qquad (2)$$

In this expression, we used the total number density, $n_{rel} = [1/(s-1)]N_0 E_{min}^{-(s-1)}$, and the mean energy, $\bar{E} = [(s-1)/(s-2)]E_{min}$ (assuming $s > 2$); C contains numerical constants. We see that the higher emissivity of the features must reflect a higher density, magnetic field or mean particle energy than in the surroundings (or a significantly different electron spectrum in the two regions).

The geometry of the features is also important. In M87, we see that many of the features tend to be linear (that is, they have one dimension longer than the other two). This includes fairly straight structures such as θ or α, and could also include "loop" features such as β or γ. Many of the lower contrast, unlabeled features—if real—also appear linear. On the other hand, some of the features appear spherical, or at least closed, structures—the "loops" could be described this way. In the absence of information on the direction of the projected magnetic field, we cannot be certain of the geometry or even the identity of many of these structures. (In Cyg A, and in the jet of M87, the projected magnetic field tends to follow the filaments, confirming their physical reality and suggesting that they are truly linear structures; Dreher, Carilli, and Perley 1987; OHC).

In this paper, we discuss several possible origins for these structures: embedded stellar objects, cooling instabilities, resistive instabilities, and transient effects such as turbulence or shocks.
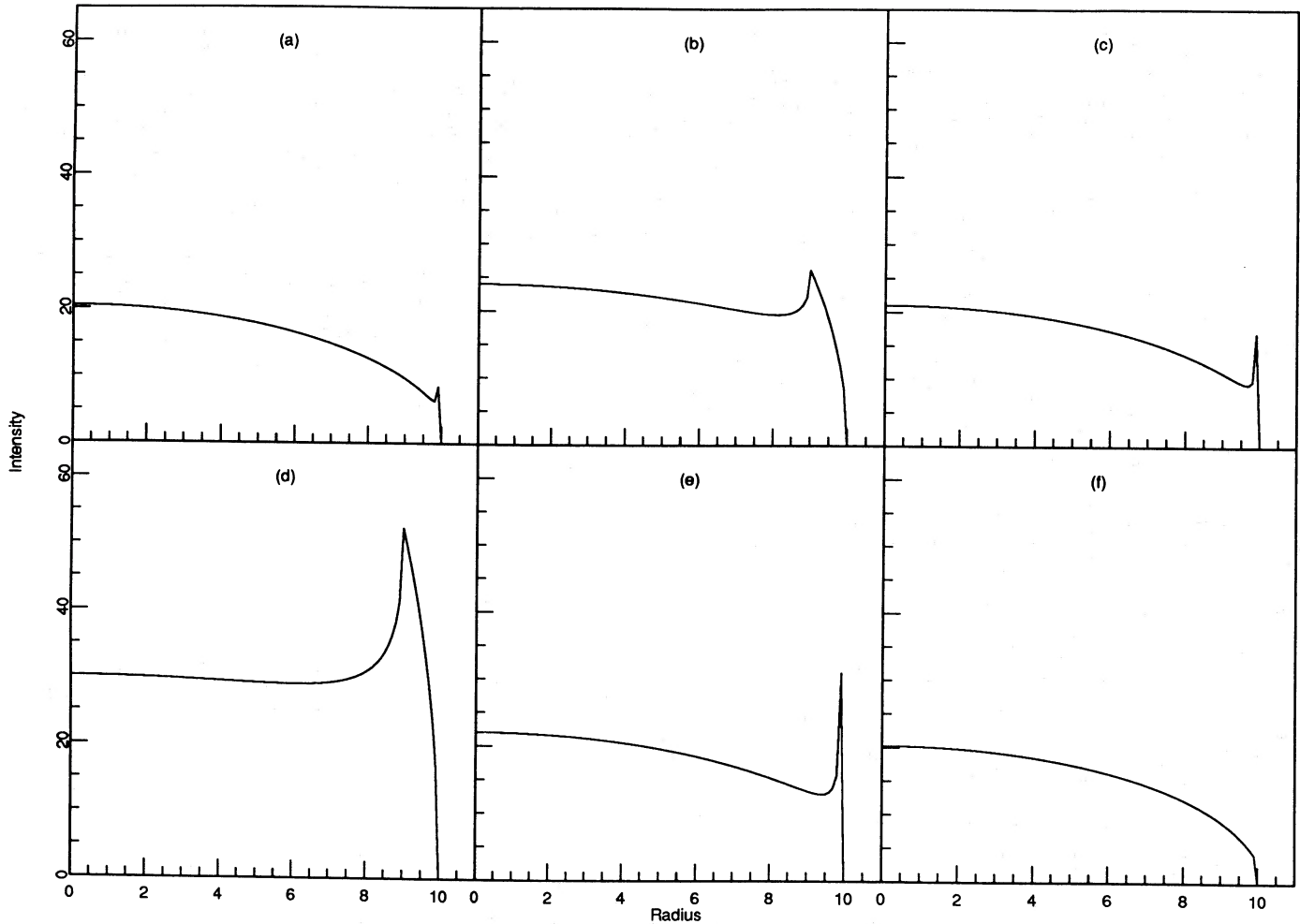
FIG. 6.—Model brightness profiles for a shell of high emissivity plasma surrounding a spherical region of lower emissivity. The fractional shell thickness (r) and emissivity (J) ratios used were (a) $r = 0.99$, $J = 2.0$; (b) $r = 0.9$, $J = 2.0$; (c) $r = 0.99$, $J = 5.0$; (d) $r = 0.9$, $J = 5.0$; (e) $r = 0.99$, $J = 10.0$; (f) $r = 0.999$, $J = 10.0$. The shell thickness ratios were chosen approximately to match the ratio of thickness of feature θ to the radius of curvature of the feature.

One possibility is that the bright features are simply due to normal stellar objects embedded in the radio source. One is led to this idea in M87, unlike the larger radio sources with filamentary structure, by the round morphology of many of the features. This idea was presented by Blandford and Königl (1979) as the origin of the knots in the jet; they proposed the jet was overrunning dense interstellar clouds or supernova remnants in the galaxy. The newer observations which reveal that the "knots" in the jet are filamentary structures (OHC) seem to disprove this idea for the jet. While the geometry of some of the features within the lobe is more consistent with such a model, we do not think the model is likely to work.

The most likely candidate object might be supernova remnants (SNRs), as they are sources of synchrotron radiation. However, the round features in M87 are both larger and brighter than typical galactic SNRs. The integrated luminosities of features β, γ, δ, ϵ, and ζ fall in the range 0.5–1.0 $\times$ 10^{39} ergs s^{-1}, and all have sizes ~ 100 pc. For comparison, typical SNRs in our Galaxy have luminosities in the range 10^{33}–10^{34} ergs s^{-1} and sizes ~ 4–10 pc (Braun, Lyne, and Goss 1989; here a spectral index $\alpha = 0.8$ was assumed to convert 6 cm fluxes to integrated luminosities). Even though differences in

ambient conditions will affect the size and radio luminosity of a supernova remnant (e.g., Dickel et al. 1989), we doubt that this large difference in size and luminosity can be accounted for by different conditions in M87 and in our Galaxy. Furthermore, we note that the work necessary to push aside a ~ 100 pc sphere of gas at a pressure $\sim 4 \times 10^{-10}$ dyn cm^{-2} is $\sim 5 \times 10^{52}$ ergs, which is greater than the total energy of a supernova ($\sim 10^{51}$ ergs; e.g., Woolsey and Weaver 1986). We therefore do not believe the round features in M87 are due to embedded SNRs.

One might argue that other, larger stellar objects might be the cause of the round features: embedded H II regions, globular clusters or molecular clouds, for instance. (It is not obvious that H II regions or molecular clouds would be found in the center of the elliptical galaxy M87, but star formation has been proposed to occur in cooling flows; Sarazin and O'Connell 1983; Silk et al. 1986). However, we do not consider this a likely picture, either. None of these objects are themselves synchrotron sources; the features in M87 would have to be due to the interaction of the radio luminous plasma with the embedded objects. Blandford and Königl (1979) suggested bow shocks in a supersonic flow as a model for the knots in the jet;
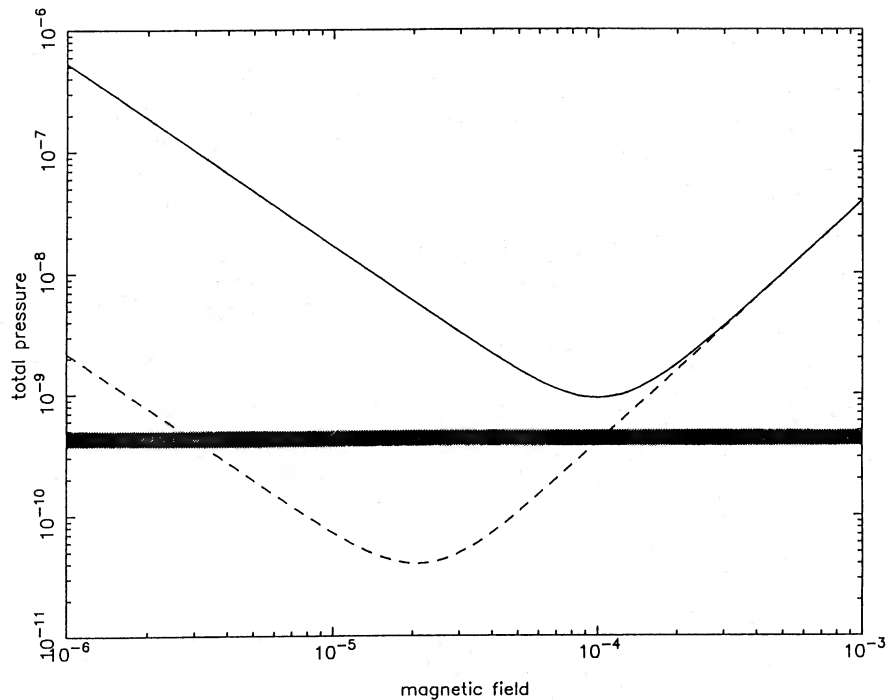
FIG. 7.—The total pressure in relativistic particles and magnetic field, as a function of magnetic field, for two values of p_{min}. The solid line is for $p_{min} = 10^{-9}$ dyn cm^{-2}, corresponding to a bright filament, with a minimum-pressure magnetic field of 100 μG. The dotted line is for $p_{min} = 4 \times 11^{-10}$ dyn cm^{-2}, corresponding to the minimum pressure value for the interfilament background. The shaded area shows the range of thermal pressures of the background X-ray gas, estimated from the White and Sarazin (1988) model, as described in the text.

we do not necessarily see evidence for supersonic flow in the lobe, nor are the round, closed shapes of many of the features consistent with a bow shock.

Finally, embedded stellar objects will not lead to linear features like those seen in M87 and which are common in larger radio galaxies. We thus do not believe embedded stellar objects can account for the features. In what follows, we consider thermal and resistive instabilities as the origin of the features. We conclude that thermal instabilities cannot account for the features, while resistive instabilities require special circumstances in order to account for them.

V. THERMAL INSTABILITIES AS THE ORIGIN OF THE FILAMENTS

One mechanism which can lead to a two-phase medium is the thermal instability, first proposed by Field (1965) and extended to relativistic plasmas by Simon and Axford (1972). These instabilities lead to dense, cool regions within a hotter external medium: the collapse is driven by the external pressure as the enhanced cooling within the higher-density perturbation reduces the internal energy of the perturbed region. Flux freezing in the collapse will increase the magnetic field in the perturbed region. The time scale for the collapse is the cooling time scale for the energetically dominant component of the plasma. A magnetized plasma is thermally unstable only if $\beta = 8\pi(p_{rel} + p_{th})/B^2 \gtrsim$ a few (the exact instability criterion depends on the details of the system; Eilek and Caroff 1979). A high-β plasma can be driven unstable either by thermal cooling (such as bremsstrahlung), if the thermal plasma dominates the internal pressure, or by synchrotron cooling if relativistic electrons dominate the internal pressure.

The smallest scale in a plasma which is thermally unstable is set by thermal conduction: small scales will find heat transported in from their surroundings by conduction more quickly

than they can radiate away their internal energy, so the instability is quenched. But the thermal conductivity across a magnetic field is much smaller than that along the field (e.g., Spitzer 1962). This suggests that linear filaments will tend to form in regions of ordered fields, but spherical condensations can grow if the field is tangled on scales smaller than the perturbation.

Throughout this section we will use the observations to constrain the density and emissivity ratios between the filaments (subscript "f") and the interfilament medium ("IFM"; subscript "i"). We will assume that conditions in the IFM are similar to the original conditions in the plasma before the instability took place. This is probably a good assumption unless the entire lobe has evolved during the growth of the instability (as in the expanding flow models of dal Pino and Opher 1989), or unless a large fraction of the mass in the lobe has gone into filaments.

a) Synchrotron Instability

This instability goes if the plasma is initially high-β, and if the pressure of the plasma is dominated by the radiating particles. The latter condition requires either that the plasma be electron-positron, or that the ions required for charge neutrality do not carry much of the internal energy. If these conditions are satisfied, an overdense perturbation will collapse on a radiative (synchrotron) time scale. The final state of the perturbation will be a cloud or filament which is supported by its enhanced magnetic pressure against the external, hot medium; the relativistic particle energy will be in large part radiated away so that the cloud is now low-β. We do not believe this instability can account for the features seen in M87. Filaments produced by a synchrotron instability are likely to be *darker* than their surroundings, not brighter. Even if local conditions

conspire to allow a filament to be bright at low frequencies, the filament spectrum will be steeper than that of the surroundings, so its observability will be a strong function of frequency. We show this as follows.

From the condition of pressure balance between the dense filament and its surroundings, we find a relation between the final and initial densities:

$$\frac{n_f}{n_i} = \left(\frac{1 + \beta_i}{1 + \beta_f}\right)^{1/2} . \tag{3}$$

From this and the definition of β (and with $p_{th} \ll p_{rel}$ in this case), we also have

$$\frac{p_f}{p_i} = \frac{\beta_f}{\beta_i}\left(\frac{1 + \beta_i}{1 + \beta_f}\right) . \tag{4}$$

Since $p = n\bar{E}$, equations (3) and (4) also relate $\bar{E}_f$ to $\bar{E}_i$. We note that $\bar{E}_f \ll \bar{E}_i$, since the electrons which supply the bulk of the internal energy must have time to cool in order for this instability to go. In particular, if the initial electron spectrum is a power law with $s > 2$, then $\bar{E} \simeq E_{min}$. The time scale on which the filament collapses is the synchrotron time scale of electrons at $\bar{E}_i$. During this cooling, the electron spectrum steepens at energies $E \gtrsim \bar{E}$, at least to $N(E) \propto E^{-(s+1)}$ (e.g., Pacholczyk 1970; this ignores pitch ange scattering during the collapse and will be the most favorable case for seeing the filaments).

Taking this spectral steepening into account, we can use equation (2) to write the emissivity ratio in terms of the initial electron spectral index as

$$\frac{j_f(v)}{j_i(v)} = \frac{n_f}{n_i}\left(\frac{B_f}{B_i}\right)^{(s+1)/2}\left(\frac{\bar{E}_f}{\bar{E}_i}\right)^{(s-1)}\left(\frac{v}{v_f}\right)^{-1/2} , \tag{5}$$

where $v_f = 3\bar{E}_f^2 B_f/4\pi m_e^3 c^5$ is the characteristic synchrotron frequency of particles at $\bar{E}_f$ in the magnetic field B_f.

We will use the fact that the initial magnetic field must be larger than the inverse Compton equivalent field, $B_{ic} = 3(1 + z)$ μG, in order for the instability to go (inverse Compton losses are thermally stable). This limits the allowed initial β_i:

$$\beta_i < \frac{8\pi p_x}{B_{ic}^2} - 1 . \tag{6}$$

For the high pressures in the center of M87, this limit becomes $\beta_i \lesssim 1100$. We also need the relationship of B to n in the collapse: flux freezing predicts $B \propto n$ in a linear collapse, and $B \propto n^{2/3}$ in a spherical collapse (as might occur in a region of tangled field). We use these relations, equations (3) and (4), and the upper limit on β_i to derive an upper limit on the emisssivity ratios. For a linear collapse,

$$\frac{j_f(v)}{j_i(v)} < 40 p_{x,10}^{(5-2s)/4} f_l(\beta_f)\left(\frac{v}{v_f}\right)^{-1/2} \tag{7a}$$

and for a spherical collapse,

$$\frac{j_f(v)}{j_i(v)} < 8 p_{x,10}^{(7-2s)/6} f_s(\beta_f)\left(\frac{v}{v_f}\right)^{-1/2} . \tag{7b}$$

Here,

$$f_l(\beta_f) = \beta_f^{(s-1)}/(1 + \beta_f)^{(3s-1)/4} ,$$

$$f_s(\beta_f) = \beta_f^{(s-1)}/(1 + \beta_f)^{(4s+1)/6} ;$$

we have assumed $\beta_i \gg 1$ and written $p_{x,10} = p_x/10^{-10}$ dyn

cm^{-2}. Now, the functions $f_l(\beta_f)$ and $f_s(\beta_f)$ have upper bounds: max $[f_l(\beta_f)] \simeq (0.40)^{(s-1)}$, for $\beta_f \sim 2$–3; max $[f_s(\beta_f)] \simeq (0.52)^{(s-1)}$, for $\beta_f \sim 3$–5. Choosing $s = 2.4$ (corresponding to a photon spectral index of 0.7 as an estimate for the interfilament plasma), and $p_x \simeq 4 \times 10^{-10}$ dyn cm^{-2} for M87, we derive the upper limit for a linear collapse,

$$\frac{j_f(v)}{j_i(v)} < 27\left(\frac{v}{v_f}\right)^{-1/2} \tag{8a}$$

and for a spherical collapse,

$$\frac{j_f(v)}{j_i(v)} < 5\left(\frac{v}{v_f}\right)^{-1/2} . \tag{8a}$$

Thus, extreme conditions ($B_i \gtrsim B_{ic}$ and the optimum value of β_f) do just allow $j_f(v) > j_i(v)$ if $v \gtrsim v_f$; but this calculation also predicts a steep spectrum for the filaments. This latter contradicts observations which suggest that the filament spectrum may be flatter than the interfilament spectrum in M87 (F. N. Owen, private communication). In addition, Table 1 shows that a typical filament-to-background ratio is $j_f/j_i \sim 10$ at 6 cm. For linear filaments, equation (8a) requires $v_f > 0.14v \sim 600$ MHz (the filaments should not be visible below this frequency). For spherical features, equation (8b) does not allow $j_f/j_i \sim 10$ for any frequency. We therefore feel it highly unlikely that the synchrotron instability is the origin of the filaments in M87.

We note that this conclusion disagrees with that of Achterberg (1989), who argues that a synchrotron cooling instability will lead to bright filaments. However, his models invoke a couple of special conditions in order to achieve this. He assumes a fairly flat electron spectrum [$N(E) \propto E^{-2}$, as from a strong shock], which extends to energies which radiate at optical frequencies. The mechanism which accelerates the electrons to this flat spectrum must avoid accelerating the ions, as mentioned above; it must also be local to the filaments, as the synchrotron lifetime of particles which radiate in the optical will be quite short. If such a flat electron spectrum is produced, it will put most of the energy density in the high-energy electrons. They will cool quickly without disturbing the low-energy spectrum, and the resulting adiabatic compression will indeed lead to bright filaments. Thus, the radio spectrum of both the filaments and the interfilament material in this model will be flat, $\propto v^{-0.5}$. Observations, however, find that both the filaments and the interfilament emission in M87 have somewhat steeper spectra than this, and that the filament spectrum may be flatter than the interfilament spectrum (F. N. Owen, private communication); this does not agree with the model. We therefore do not feel that synchrotron cooling explains the filaments in this source.

b) Bremsstrahlung Instability

Having argued that the pure synchrotron instability does not work, we might consider an alternative: a relativistic particle population mixed in with and dynamically tied to the thermal plasma in the core of M87. This might occur in M87 if, for instance, the jet entrained thermal gas before entering the lobe, or if the relativistic particles which fill the lobe have diffused into the thermal gas. If this mixed plasma is dominated by the thermal gas pressure, so that $p_{th} > p_{rel} + p_B$ (which is consistent, we note, with our value of the minimum pressure in the interfilament background of the inner lobes, as in Table 2),

the thermal instability will simply be driven by the bremsstrahlung losses of the thermal gas.

This instability goes on the thermal cooling time,

$$t_{th} \simeq 1.0 \times 10^7 \frac{T_7^{1/2}}{n_{th}} \text{ yr} . \tag{9}$$

We normalize the temperature as $T_7 = T/10^7$ K; we keep the density in units of cm^{-3}. The synchrotron lifetime of the particles which initially (before collapse) radiated at a frequency ν in the initial magnetic field B_i is

$$t_{sy} \simeq 1.1 \times 10^9 \frac{1}{B_{i,\mu G}^{3/2} \nu_{GHz}^{1/2}} \text{ yr} . \tag{10}$$

If $t_{sy} > t_{th}$, the relativistic particles will be adiabatically compressed in the collapsing perturbation. Due to the increased magnetic field, density, and relativistic particle energy in the collapse, the dense perturbation will have a higher synchrotron emissivity than the background. Thus, this mechanism can in principle lead to bright clouds or filaments in radio sources. However, this model does not work quantitatively for M87, for reasons which we present in the rest of this section.

To start, we use the observations to estimate the density ratio between the filaments and the IFM. As before, we assume the IFM conditions have not changed much from the conditions before the instability started. Now, in an adiabatic collapse, the mean relativistic particle energy $\bar{E} \propto n^{1/3}$. Thus, from equation (2), the synchrotron emissivity $j_{sy} \propto n^{(5s+7)/6}$ in a linear collapse, and $j_{sy} \propto n^{(2s+3)/3}$ in a spherical collapse. Thus, as s varies between 2 and 3, j_{sy} varies as $n^{2.8}$ to $n^{3.7}$ in a linear collapse, and as $n^{2.3}$ to $n^{3.0}$ in a spherical collapse.

From Table 1 we can choose a filament-to-background emissivity radio, $j_f/j_i \sim 10$. This gives us a density ratio $n_f/n_i \sim 2$ in a linear geometry, and $n_f/n_i \sim 2.5$ in a spherical geometry, for the expected range of s.

With this, we can check the consistency of our adiabatic assumption. If we require $t_{sy} > t_{th}$, equations (9) and (10) show that conditions in the initial plasma must satisfy

$$B_i < 22 \left(\frac{n_{th}}{T_7^{1/2} \nu_{i,GHz}^{1/2}} \right)^{2/3} \mu G . \tag{11}$$

Following OHC and using the scaled White and Sarazin (1988) model to estimate the density and temperature of the precollapse plasma at $n_{th} \sim 0.15$ cm^{-3} and $T \sim 3 \times 10^7$ K, this limit becomes

$$B_i < 4.3 \nu_{i,GHz}^{-1/3} \mu G . \tag{12}$$

This limit will be more useful if we express it in terms of conditions in the collapsed filament. We have $B_f \sim 2B_i$ in either geometry. The frequency at which a particle radiates most of its energy is $\nu \propto E^2 B \propto n^{5/3}$ (linear) or $n^{4/3}$ (spherical). Thus, particles which we observe at 4.8 GHz must have radiated at 1.5 GHz (linear) or 1.9 GHz (spherical) before the collapse. A tighter constraint, however, comes from the fact that at least the brighter features (θ, η) are detected at 15 GHz and show no evidence of spectral steepening between 1.4 and 15 GHz (F. N. Owen, private communication). The electrons which we see at 15 GHz must have radiated at 4.7 GHz (linear) or 6.0 GHz (spherical) before the collapse. The 4.8 GHz values limit the magnetic field in the bright features to $B_f < 7.5$ μG (linear) or 7.0 μG (spherical); the 15 GHz values require $B_f < 5.1$ μG (linear) or 4.7 μG (spherical).

This limit has two consequences. First, $B_f \ll B_{\min p}$ and $B_f^2 \ll 8\pi p_{th}$. Thus, the filaments must be supported by relativistic particle pressure. Pressure balance between the filaments and the IFM gives $p_{rel,f} \simeq p_{th,i} + p_{rel,i}$. But we know that $p_{rel} \propto n^{4/3}$. We can thus relate the thermal and relativistic particle pressures before the collapse:

$$p_{th,i} \simeq p_{rel,i} \left[\left(\frac{n_f}{n_i} \right)^{4/3} - 1 \right] . \tag{13}$$

This gives us $p_{rel,i} \simeq 0.66 p_{th,i}$ (linear) or $p_{rel,i} \simeq 0.42 p_{th,i}$ (spherical). Either geometry requires the relativistic particle pressure to be a significant part of the thermal pressure before the collapse.

The second consequence of equation (11) is apparent from Figure 7. We see that $B < B_f \ll B_{\min p}$ requires $p \gg p_{\min}$; if $B_f \lesssim 0.1 B_{\min p}$, as we find in M87, $p \gtrsim 30 p_{\min}$. This pressure is well above the pressure of the thermal gas. Thus, thermal confinement does not seem possible for this description of the filaments. But this invalidates the fundamental assumption of the model, that the filaments arose from a thermal instability, since this instability leads to dense regions which are in pressure balance with their surroundings.

Another consequence of these constraints on conditions in the initial plasma is that thermal conduction appears likely to preclude the instability occurring at all. To demonstrate this, we recall the size scales which are unstable in a linear, homogeneous thermal instability analysis (see Eilek and Caroff 1979). The largest unstable scale is $\lambda_{max} \sim c_s t_{th}$ if c_s is the sound speed in the plasma. For the conditions in the core of M87, $\lambda_{max} \sim 4 T_7/n_{th}$ kpc ~ 80 kpc for the conditions in the region.

The smallest unstable scale is that on which thermal conduction of heat from the hot plasma outside the cooling region can balance the radiative losses. If q is the conductive heat flux and $j_b \simeq 1.4 \times 10^{-27} n_{th}^2 T^{1/2}$ ergs s^{-1} is the bremsstrahlung emissivity, this balance occurs when

$$j_b \simeq \nabla q \sim \frac{q}{\lambda_{min}} . \tag{14}$$

This determines λ_{min}. The heat flux in the mixed plasma will be carried both by the thermal gas and the relativistic particles. Consider conduction along magnetic field lines. The thermal heat flux is

$$q_{th} = \kappa_{\parallel} \nabla (k_B T) , \tag{15}$$

where $\kappa_{\parallel} = 20(2/\pi)^{3/2}(k_B T)^{5/2}/m_e^{1/2} e^4 \ln \Lambda$ is the parallel thermal conductivity; $\ln \Lambda$ is the Coulomb logarithm (Spitzer 1962). The relativistic particles are collisionless, so we cannot find their heat flux from an expression like equation (15), which is based on particle-particle collisions. Rather, we follow Cowie and McKee (1977) who write the heat flux in this "saturated" limit as

$$q_{rel} \simeq \zeta p_{rel} c . \tag{16}$$

Here, ζ is a numerical factor less than unity (Cowie and McKee use $\zeta = 0.4$ for nonrelativistic particles) and we have taken the characteristic velocity of the particles as lightspeed.

By comparing equations (15) and (16), we see that the relativistic particles dominate the heat flux on scales

$$\lambda \gtrsim \lambda_{crit} \simeq \frac{\kappa_{\parallel}}{\zeta c} \frac{1}{n_{th}} \frac{p_{th}}{p_{rel}} . \tag{17}$$

But with our estimate of density and temperature, and assuming $\zeta \ln \Lambda \sim 10$, we find $\lambda_{\rm crit} \simeq 0.05 p_{\rm th}/p_{\rm rel}$ kpc. Since $p_{\rm th} \sim 2 p_{\rm rel}$ is required from equation (13), the relativistic particle heat flux will be the strongest stabilizing effect for scales of interest (and in fact the $\lambda_{\rm min}$ estimated from $q_{\rm rel}$ is much larger than this $\lambda_{\rm crit}$).

We therefore estimate the minimum unstable scale from equation (14): $\lambda_{\rm min} \sim q_{\rm rel}/j_b$. For our temperature and density values this is $\lambda_{\rm min} \sim 3 p_{\rm rel, -10}$ Mpc (we have normalized $p_{\rm rel}$ to 10^{-10} dyn cm^{-2}). This very large number (in fact, $\lambda_{\rm min} > \lambda_{\rm max}$) means that the strong relativistic particle thermal conduction will quench *all* field-aligned thermal instabilities in this environment.

This argument addressed field-aligned conduction; heat conduction across an ordered magnetic field is dramatically reduced, and perturbations much smaller than a Mpc which are oriented across the field can probably grow, at least formally. But a very special, very ordered magnetic field geometry would be necessary to vitiate the argument above and allow three-dimensional perturbations to grow. For instance, a fully disordered, tangled field will only reduce the thermal conductivity by a factor of $\frac{1}{3}$ over the field-aligned value (Hollweg and Jokipii 1972), so this geometry will not help the model. One would need a magnetic field which was not connected to the outside of the feature at all, sort of a self-contained magnetic "bubble"; a linear filament would not work, as heat conduction would flow along the filament.

Thus, we do not believe that cooling instabilities can be responsible for the bright filaments in the inner lobes of M87. However, it is interesting to apply the argument above to the optical filaments which lie north of the radio lobes. These features lie outside of the inner radio lobes at a similar distance from the core as the radio filaments. The relativistic particle pressure to which the optical filaments are exposed will be that of the diffuse, $\sim 12'$ halo. This $p_{\rm rel}$ might be estimated from the equipartition magnetic field (4 μG) of Andernach *et al.* (1979). With this, equation (17) leads to $\lambda_{\rm crit} \sim 3$ kpc, while equations (14) and (15) give $\lambda_{\rm min} \sim 9$ kpc. Since these estimates, especially $p_{\rm rel}$ from equipartition, but also the density and temperature model fits, are probably not exact, it is possible that $\lambda_{\rm crit} \sim \lambda_{\rm min} \sim$ few kpc. This may suggest that the relativistic particle pressure is low enough to allow the instability to go in the halo, while the higher $p_{\rm rel}$ quenches the instability in the radio lobe. This might be related to the way the optical filaments appear to "avoid" the inner radio lobes.

Finally, we note that the larger question of thermal instability in cooling flows is complex. The homogeneous, linear stability analysis—from which we have argued here—may not apply to large-scale instabilities in the gravitational potential of clusters of galaxies (Balbus 1988). Further, neither dynamically important magnetic fields nor transonic flows have been included in cooling-core stability analysis, yet there is evidence for both phenomena in the Virgo core (Owen and Keel 1989; Owen, Eilek, and Keel 1989). Thus these last comments can be no more than speculative.

VI. TEARING INSTABILITIES AS THE ORIGIN OF THE FILAMENTS

This instability is caused by the tendency of a diffuse current to filament, due to the self-attraction of parallel currents. It was first considered by Furth, Kileen, and Rosenbluth (1963); see also Bateman (1978). The filamentation is allowed by the presence of non-zero resistivity, which violates the usual flux-freezing assumption and allows the magnetic field lines to move through the plasma and bunch together. This process is observed in current sheets in laboratory plasmas and in numerical simulations, where magnetic islands and current filaments are indeed found: high-field regions immersed in a low-field background. Examples can be found in Colgate (1978), Furth (1985, Fig. 12) and in the numerical simulations of Matheus and Montgomery (1981). OHC suggest this instability as the most likely origin of the luminous filaments seen in the jet of M87.

Tearing instabilities lead to ordered, high-field regions surrounded by regions of low field strength. Both theoretical calculations and computer simulations suggest that the tearing mode in a flat current sheet will saturate when the filaments are not too much larger than the size of the boundary layer (see Bateman 1978 or Furth 1985). The final state of the filaments may well be self-contained, and possibly self-confined structures (where self-confined means the magnetic field *locally* confines the plasma). The magnetic flux ropes seen in the atmosphere of Venus (Russell and Elphic 1979) are examples of structures that are observed to be locally self-confined magnetoplasma systems. It has also been suggested that the "plasmoids" observed in the Earth's magnetotail during substorms are self-confined spheroidal systems, perhaps similar to the spheromak structures created in the laboratory (Hones 1985).

We can test this idea by looking at the growth rate of the instability. Since resistivity is necessary, the plasma is highly conductive and the scales are large, we might expect the growth to be very slow. The linear analysis of Furth, Kileen, and Rosenbluth (1963) considers a flat current sheet of width a in a cool plasma (where $\nabla p \ll [(\nabla \times \boldsymbol{B}) \times \boldsymbol{B}]/4\pi$ in the current sheet). Following them, we define the Alfvén wave crossing time,

$$t_{\rm A} = a/v_{\rm A} , \qquad (18)$$

if $v_{\rm A} = B/(4\pi\rho)^{1/2}$ is the alfvén speed (ρ is the mass density), and the resistive diffusion time,

$$t_r = 4\pi a^2/\eta , \qquad (19)$$

where $\eta = c^2/\sigma$ is the resistive diffusivity (σ is the electrical conductivity). The tearing mode is unstable for all scales $\gtrsim a$. The fastest growth rate is for perturbations of scale of $\sim a$. Their growth time, in the limit $t_r \gg t_{\rm A}$, is

$$t_{\rm tear} = t_r^{3/5} t_{\rm A}^{2/5} . \qquad (20)$$

We see that this is an intermediate time scale: $t_{\rm A} < t_{\rm tear} < t_r$.

In order to estimate this growth time we need the value of η (or σ). The simple, Coulomb conductivity is very large (see Spitzer 1962), and the resultant $t_{\rm tear}$ for scales comparable to the filaments in M87 would be too long to be of interest. However, the resistivity in a thin current sheet is often anomalous, arising from particle interactions with plasma turbulence rather than the much less frequent particle-particle collisions (e.g., Spicer 1982). A detailed model of the plasma turbulence would be necessary to determine the magnitude of the resistivity. Instead we use a simple upper limit which can be found for anomalous resistivity, as follows.

The resistive diffusivity can be written in terms of the electron collision rate, ν_e, as

$$\eta = \frac{\bar{E}}{n_e e^2} \nu_e \qquad (21)$$

(e.g., Lifshitz and Pitaevskii 1981); $\bar{E} = \bar{\gamma} m_e c^2$ is the average energy per electron. The anomalous collision rate is unknown, but an extreme upper limit (e.g., Papadopoulos 1977) should be the plasma frequency: $v_e \lesssim \omega_{pe}/2\pi$, where $\omega_{pe}^2 = 4\pi n_e e^2/\bar{\gamma} m_e$ for a (possibly) relativistic plasma (e.g., Gould 1981). Combining these we have an upper limit to η:

$$\eta \lesssim \frac{2c^2}{\omega_{pe}} \sim 3.2 \times 10^{22} \left(\frac{\bar{\gamma}}{n_e}\right)^{1/2} \text{cm}^2 \text{ s}^{-1} . \qquad (22)$$

This gives us a lower limit on the growth time. From equations (12), (13), and (14) we get as a general expression,

$$t_{\text{tear}} \gtrsim \frac{(2\pi\omega_{pe})^{3/5} a^{8/5}}{(c^3 v_A)^{2/5}} \simeq 4.8 \times 10^{10} \frac{a_{\text{pc}}^{8/5} n_e^{1/2}}{B_{\mu G}^{2/5} \bar{\gamma}^{3/10}} \text{ yr} . \qquad (23)$$

Here we have scaled the width of the current layer, a, in pc, and B in μG; n is in cm^{-3}; and we have assumed an electron-ion plasma in evaluating v_A. We emphasize that $\bar{\gamma}$ in equation (23) is the mean electron Lorentz factor. If the electrons have a power-law spectrum with spectral index $s > 2$, then $\bar{\gamma} \simeq \gamma_{\min}$. If the plasma is dominated by thermal, subrelativistic electrons, then $\bar{\gamma} \simeq 1$.

Now, equation (23) tells us immediately that this instability is very slow in the high density ($n \gtrsim 0.1$ cm^{-3}), thermal plasma surrounding the radio source. For instance, if $B \sim 10$ μG, $t_{\text{tear}} \gtrsim 6a_{\text{pc}}^{8/5}$ Gyr. The width of the current layer is of course unknown. The fact that some of the features are resolved at $\gtrsim 0\rlap{.}{''}4 \sim 30$ pc, suggests that the initial current sheet must not have been thinner than $a \sim 10$ pc or so. Thus, if the radio-luminous relativistic plasma from the jet is well mixed with the surrounding gas, this instability cannot account for the bright features.

On the other hand, we can consider this instability in a low-density, relativistic plasma—which might describe the jet plasma. This will shorten t_{tear} by reducing n_e and increasing $\bar{\gamma}$. We find, however, that this instability is still slow. The lowest limit on the density is that of the radiating electrons themselves. The inner lobes are detected at frequencies as low as 100 MHz (e.g., Graham 1970). The particle energy which radiates at this frequency is $\gamma \simeq 2400/B_{\mu G}^{1/2}$. If we identify this with the mean particle energy, $\bar{\gamma}$ (an assumption which gives the lowest limit for n_e), we have $n_e \gtrsim 3p_{\text{rel}}/\bar{\gamma} m_e c^2 \simeq 5 \times 10^{-7} p_{\text{rel}, -9} B_{\mu G}^{1/2}$ cm^{-3}. (Here we have scaled p_{rel} to 10^{-9} dyn cm^{-2}, thinking of the jet; e.g., OHC). Using this estimate for the density in equation (23) allows us to put a lower limit on t_{tear} in M87, for the case where only relativistic electrons contribute to the density:

$$t_{\text{tear}} \gtrsim 3.4 \times 10^6 a_{\text{pc}}^{8/5} p_{\text{rel}, -9}^{1/2} \text{ yr} . \qquad (24)$$

Thus, a tearing instability might go in the relativistic jet plasma within the lifetime of the source. However, this limit is very optimistic; we have taken $v_e \lesssim \omega_{pe}/2\pi$ and assumed that only relativistic electrons radiating at or above 100 MHz contribute to the number density. Any loading of the plasma with cooler electrons, or any reduction of the resistivity from the optimum value, equation (22), will increase the limit in equation (24).

In addition, this estimate of t_{tear} should be compared to the synchrotron cooling time, equation (10). In order for the filaments to form before the highest energy electrons have cooled, we must use the highest frequency at which the inner lobes have been observed, namely 23 GHz (Forster 1980). (This frequency corresponds to electrons with energy $\gamma \simeq 3.6 \times 10^4/B_{\mu G}^{1/2}$). Combining this with the lower limit for t_{tear}, we

find that $t_{\text{tear}} < t_{\text{sy}}$ if

$$a_{\text{pc}}^{8/5} p_{\text{rel}, -9}^{1/2} B_{\mu G}^{3/2} < 64 . \qquad (25)$$

In the jet of M87, $p_{\text{rel}, -9} \gtrsim 1$ (OHC), so $a_{\text{pc}}^{16/15} B_{\mu G} \lesssim 16$ is needed in order to have $t_{\text{tear}} < t_{\text{sy}}$. We argued above that $a \sim 10$ pc might be a decent estimate for the thickness of the current sheet; (25) then requires $B \lesssim 1$ μG for the instability to go in one synchrotron time. This might be considered just plausible, since this condition refers to the preinstability field; but the fact that very optimistic assumptions were used in deriving t_{tear} make this seem unlikely. (Additionally, assuming $B^2 \ll 8\pi p$ invalidates the assumption of a cold plasma which was used in deriving the basic growth rate).

We also note that this situation is not helped appreciably if the jet plasma is electron-positron, rather than electron-ion. In this case, the Alfvén speed is likely to be $v_A \simeq c$, and the condition which replaces (25) is $a_{\text{pc}}^{8/5} p_{\text{rel}, -9}^{3/10} B_{\mu G}^{9/5} < 860$. Although this slightly eases the constraints discussed above, it is still a rather tight constraint on the system.

Thus, even the most favorable estimates of the tearing growth rate cannot produce filaments in less time than the synchrotron loss time of the highest energy electrons seen. *In situ* particle acceleration within the filaments might offset this problem. Local acceleration is certainly possible in the currents which flow along filaments (e.g., Spicer 1982). We do not present the detailed model which would be needed to incorporate acceleration into this argument. We just note that in situ acceleration might relax the instability condition to the requirement that t_{tear}, estimated from equation (24), be less than the age of the source.

VII. WHAT ABOUT TRANSIENT EFFECTS?

We have seen that cooling instabilities cannot account for the bright features in the inner lobes of M87. Resistive instabilities are unlikely to account for the features unless *in situ* reacceleration of the electrons takes place.

A different possibility is that the bright features might be transient rather than long-lived phenomena. For instance, one might suspect that the plasma is turbulent, and that the brightness fluctuations are local regions of high density and magnetic field within the turbulence. The numerical simulations of three-dimensional MHD turbulence by Menguzzi, Frisch, and Pouquet (1981) find that the magnetic field tends to be high in fairly large, isolated regions within the system. This might give the appearance of quasi-discrete features as in M87. Spangler (1982) and Eilek (1989) have suggested that fluctuations in total and polarized intensity might be due to turbulence. However, we do not think that simple MHD turbulence can account for the brighter features in M87. The problem is the strength of the emissivity contrast. For subsonic MHD turbulence, with magnetic field fluctuation amplitude B_t and turbulent "cell" size λ_t, in a region of overall scale L and ordered magnetic field B_0, the fractional surface brightness fluctuation will be $\sim [B_t^2 \lambda_t/(B_0^2 + B_t^2)L]^{1/2}$ (Eilek 1989). This is a small quantity for normal, low-amplitude turbulence, in which $B_t \lesssim B_0$ and $\lambda < L$, so that one expects no more than, say, 10% fluctuations. The lower contrast, unlabeled, features may be due to such turbulence; but the higher contrast, labeled features seem unlikely to be caused by this mechanism. (Another way to see this is to note that the emissivity contrast in the bright filaments requires both density and magnetic field

enhancements of a factor ~ 2. This does not happen in subsonic turbulence).

Another phenomenon possibly related to turblence is the appearance of luminous filaments in the numerical simulations of Norman, Clarke, and Burns (1988). These authors included a passive magnetic field ($B^2/8\pi \ll p$) in their simulations of supersonic two-dimensional jets, and the synchrotron emission from "fingers" of jet fluid in the turbulent mixing layer resemble the features seen in M87 or other radio sources. However, we do not think this can account for the filamentary features in M87. To see this, recall that features which are far from equipartition between magnetic and plasma pressures, as is the case for the passive magnetic field in the simulations of Norman, Clarke, and Burns, have internal pressures which must be well above $p_{\min}$ (e.g., Fig. 7). But since the "fingers" and "interfinger material" in the simulations are in approximate pressure balance, radio observations of the "fingers" would find $p_{\min} \ll p_{\text{ext}}$. This contradicts our data on the filaments in M87, for which $p_{\min} \gtrsim p_x$. Thus, unless there exist flows in the innerlobes which are strongly supersonic, so that the interfilament pressure can be well above that of the external gas, we do not think that these simulations are relevant for the bright features in M87.

Returning to more general turbulent models, the high emissivity contrast of the bright features seems to require strong turbulence, in which both the density and magnetic field have large amplitude fluctuations, or even shocks. In addition to the strong local density and magnetic field enhancements in shocks, the possibility of particle acceleration in the shocks could enhance the emissivity even more. Both shocks and strong turbulence are likely to be very dissipative and thus to require continual driving and energy input.

The most likely driving mechanism for strong turbulence or shocks in the lobes is the jet, which may well enter the lobe supersonically. For instance, assume the jet material is well mixed with the local thermal plasma by the time it enters the lobe. If it starts at a velocity v_j in the jet, it will have decelerated to a velocity $v_{\text{lobe}} \simeq v_j r_j n_j^{1/2}/r_{\text{lobe}} n_{\text{th}}^{1/2}$ (from momentum conservation) when it enters the lobe. Requiring $v_{\text{lobe}} \sim 500$ km s^{-1} (the sound speed in a 3×10^7 K gas), $n_{\text{th}} \sim 0.15$ cm^{-3} and $v_j \sim 0.3c$ (from Reid et al. 1989) means the jet density must be $n_j \sim 1 \times 10^{-3}$ cm^{-3} before entrainment. This is not a very restrictive limit; any lower density would lead to a higher velocity for the jet plasma when it enters the lobe.

Thus, it seems likely that the lobe material is continually being stirred by a transonic or supersonic flow where the jet bends and enters the lobe. This could lead to large amplitude density and magnetic field fluctuations, either within the turbulent lobe itself, or at the boundary where the transonic flow hits the surrounding medium. If this is the case, transient features or shocks may be the origin of the bright features in M87.

VII. CONCLUSIONS

We have presented new 6 cm radio observations of the inner core source of M87. The radio map has a dynamic range $\sim 1.5 \times 10^5$. We find that the inner radio lobes are not uniformly filled, but that much of the emission comes from discrete knots or filaments. A minimum pressure analysis finds that the minimum pressure of many of the features is comparable with that of the surrounding thermal (X-ray) gas; a few have minimum pressures somewhat greater than the external pressure.

We found that thermal instabilities cannot be the origin of these features. Thermal instabilities driven by synchrotron radiation of the relativistic electrons will lead to dark rather than bright features. A cooling instability driven by bremsstrahlung cooling of the thermal gas, with relativistic electrons tied to the gas and compressed adiabatically, might lead to bright features. However, in order for this to work in M87, the actual internal pressure of the features must be well above the observationally determined minimum pressure; this contradicts the pressure-balance assumption inherent in thermal stability analysis. In addition, the high relativistic particle pressure in the M87 environment will quench this instability by thermal conduction.

We considered whether the features might be due to a restive, tearing mode instability. We found that, under very optimistic assumptions, the growth time for the tearing mode can be short compared to the age of the galaxy (say, $t_{\text{tear}} \sim 10^8$ yr; see eq. [17]). However, we found that t_{tear} is very unlikely to be shorter than the synchrotron lifetime of the particles radiating at high frequencies; in situ reacceleration is needed to make bright features with this model.

While in situ reacceleration is possible in a current carrying filament, we feel that the need for the most favorable assumptions possible makes this model less than convincing. We therefore conclude that the bright features in M87 are likely to be transient, being strong density and magnetic field fluctuations either in shocks or in transonic turbulence. If this is the case, the bright features could either be internal to the lobes—if supersonic turbulence is driven throughout the lobes by the jet—or on the surface, if they trace irregularities in a bounding shock.

REFERENCES

Achterberg, A. 1989, Astr. Ap., submitted.
Andernach, H., Baker, J. R., von Kap-herr, A., and Wielebinski, R. 1979, Astr. Ap., 74, 93.
Baade, W., and Minkowski, R. 1954, Ap. J., 119, 221.
Baars, J. W. M., Genzel, R., Pauliny-Toth, I. I. K., and Witzel, A. 1977, Astr. Ap., 61, 99.
Balbus, S. 1988, Ap. J., 328, 395.
Bateman, G. 1978, MHD Instabilities (Cambridge: MIT Press).
Biretta, J. A., Owen, F. N., and Cornwell, T. J. 1989, Ap. J., submitted.
Biretta, J. A., Owen, F. N., and Hardee, P. E. 1983, Ap. J. (Letters), 224, L27.
Blandford, R. D., and König, A. 1979, Ap. Letters, 20, 15.

Braun, R., Gull, S. F., and Perley, R. A. 1987, Nature, 327, 395.
Braun, R., Lyne, P., and Goss, M., 1989, Ap. J., in press.
Burbidge, G. R. 1956, Ap. J., 124, 416.
Burns, J. O., Owen, F. N., and Rudnick, L. 1979, A.J., 84, 1683.
Canizares, C. R., Clark, G. W., Jernigan, J. G., and Markert, T. H. 1982, Ap. J., 262, 33.
Canizares, C. R., Clark, G. W., Markert, T. H., Berg, C., Smedira, M., Bardas, D., Schopper, H., and Kalata, K. 1979, Ap. J. (Letters), 234, L33.
Clark, B. G. 1980, Astr. Ap., 89, 399.
Colgate, S. A. 1978, Ap. J., 221, 1968.
Conway, J., Cornwell, T. J., and Wilkinson, P. N. 1989, in preparation.

Cornwell, T. J. 1986, in *NRAO Synthesis Imaging Workshop*, ed. R. A. Perley, F. R. Schwab, and A. H. Bridle (Green Bank: NRAO).
Cowie, L. L., and McKee, C. P. 1977, *Ap. J.*, **211**, 135.
Curtis, H. D. 1918, *Pub. Lick Obs.*, **13**, 31.
dal Pino, E., and Opher, R. 1989, *Ap. J.*, **342**, 686.
Dickel, J. S., Eilek, J. A., Jones, E. P., and Reynolds, S. R. 1989, *Ap. J. Suppl.*, **20**, 497.
Dreher, J. W., Carilli, C. L., and Perley, R. A. 1987, *Ap. J.*, **316**, 611.
Eilek, J. A. 1989, *A.J.*, **98**, 244.
Eilek, J. A., and Caroff, L. J. 1979, *Ap. J.*, **233**, 463.
Fanaroff, B. L., and Riley, J. M. 1974, *M.N.R.A.S.*, **167**, 31p.
Feigelson, E. D., Wood, P. A. D., Schreier, E. J., Harris, D. E., and Reid, M. J. 1987, *Ap. J.*, **312**, 101.
Field, G. B. 1965, *Ap. J.*, **142**, 531.
Ford, H. C., and Butcher, H., 1979, *Ap. J. Suppl.*, **41**, 151.
Forster, J. R. 1980, *Ap. J.*, **238**, 54.
Furth, H. P. 1985, *Phys. Fluids*, **26**, 1595.
Furth, H. P., Kileen, J., and Rosenbluth, M. N. 1963, *Phys. Fluids*, **6**, 459.
Gould, R. J. 1981, *Phys. Fluids*, **24**, 102.
Graham, I. 1970, *M.N.R.A.S.*, **149**, 319.
Hogbom, J. 1974, *Ap. J. Suppl.*, **15**, 417.
Hollweg, J. V., and Jokipii, J. R. 1972, *J. Geophys. Res.*, **77**, 3311.
Hones, E. W. 1985, *Australian J. Phys.*, **98**, 981.
Laing, R. 1980, *M.N.R.A.S.*, **193**, 427.
Lea, S. M., Mushotsky, R., and Holt, S. S. 1982, *Ap. J.*, **262**, 24.
Lifshitz, E. M., and Pitaevskii, L. P. 1981, *Physical Kinetics* (Oxford: Pergamon).
Matheus, W. H., and Montgomery, D. 1981, *J. Plasma Phys.*, **25**, 11.
Menguzzi, M., Frisch, U., and Pouquet, A. 1981, *Phys. Rev. Letters*, **47**, 1060.
Nieto, J.-L., and Lelievre, G. 1982, *Astr. Ap.*, **109**, 95.
Norman, M. L., Clarke, D., and Burns, J. O. 1988, in *Magnetic Fields and Extragalactic Objects*, ed. E. Asseo and D. Gresillon (France: Editions de Physique).

O'Dea, C. P., and Owen, F. N. 1987, *Ap. J.*, **316**, 95.
O'Donoghue, A. 1989, Ph.D. thesis, New Mexico Tech.
Owen, F. N., Eilek, J. A., and Keel, W. 1989, *Ap. J.* submitted.
Owen, F. N., Hardee, P. E., and Bignell, R. C. 1980, *Ap. J. (Letters)*, **239**, L11.
Owen, F. N., Hardee, P. E., and Cornwell, T. J. 1989, *Ap. J.*, **340**, 698 (OHC).
Owen, F. N., and Keel, W. 1989, in preparation.
Pacholczyk, A. G. 1970, *Radio Astrophysics* (New York: Freeman).
Papadopoulos, K. 1977, *Rev. Geophys. Space Phys.*, **15**, 113.
Pearson, T. J., and Readhead, A. C. S. 1984, *Ann. Rev. Astr. Ap.*, **22**, 97.
Perley, R. A., Dreher, J. W., and Cowan, J. J. 1984, *Ap. J. (Letters)*, **285**, L35.
Reid, M. J., Biretta, J. A., Junor, W., Spencer, R., and Muxlow, T. 1989, *Ap. J.*, **336**, 112.
Russell, C. T., and Elphic, R. C. 1979, *Nature*, **279**, 616.
Sarazin, C. L., and O'Connell, R. W. 1983, *Ap. J.*, **268**, 557.
Schmitt, J. H. M. M., and Reid, M. J. 1985, *Ap. J.*, **289**, 120.
Silk, J., Djorgovski, S., Wyse, R. F. G., and Bruzal, G. 1986, *Ap. J.*, **307**, 415.
Simon, M., and Axford, W. L. 1972, *Ap. J.*, **150**, 105.
Spangler, S. A. 1982, *Ap. J.*, **261**, 310.
Spencer, R. E., and Junor, W. 1986, *Nature*, **321**, 753.
Spicer, D. S. 1982, *Space Sci. Rev.*, **31**, 351.
Spitzer, L. 1962, *Physics of Fully Ionized Gases* (New York: Wiley Interscience).
Stewart, G. C., Canizares, C. R., Fabian, A. C., and Nulsen, P. E. J. 1984, *Ap. J.*, **278**, 536.
Thompson, A. R., Clark, B. G., Wade, C. M., and Napier, P. J. 1980, *Ap. J. Suppl.*, **44**, 151.
Turland, B. D. 1975, *M.N.R.A.S.*, **170**, 281.
Walker, W. C., Benson, J. M., and Unwin, S. C. 1987, *Ap. J.*, **316**, 546.
White, R. E., III, and Sarazin, C. L. 1988, *Ap. J.*, **335**, 688.
Wilkinson, P. N., Conway, J., and Biretta, J. 1987, in *IAU Symposium 129, The Impact of VLBI on Astrophysics and Geophysics*, ed. M. J. Reid and J. M. Moran (Dordrecht: Reidel), p. 509.
Woolsey, S. E., and Weaver, T. A. 1986, *Ann. Rev. Astr. Ap.*, **24**, 205.

JEAN A. EILEK: Physics Department and Astrophysics Research Center, New Mexico Tech, Socorro, NM   87801

DEAN C. HINES: Department of Astronomy, University of Texas, Austin, TX   78712

FRAZER N. OWEN: National Radio Astronomy Observatory, P.O. Box 0, Socorro, NM   87801